On the BER Performance of RIS-Enhanced NOMA-Assisted Backscatter Communication under Nakagami-m Fading

Muhammad Usman*, Sarah Basharat*, Haris Pervaiz†, Syed Ali Hassan*, and Haejoon Jung‡
*School of Electrical Engineering and Computer Science (SEECS), NUST, Pakistan
†School of Computing and Communications, Lancaster University, U.K
‡Dept. of Electronic Engineering, Kyung Hee University, Yongin, South Korea
Email: {musman.bee18seecs, sarah.phdee21seecs, ali.hassan}@seecs.edu.pk,
h.b.pervaiz@lancaster.ac.uk, haejoonjung@khu.ac.kr

***Abstract*—Backscatter communication (BackCom) has been envisioned as a prospective candidate for enabling the sustained operation of battery-constrained Internet-of-Things (IoT) devices. This approach involves the transmission of information by a backscatter node (BSN) through passive reflection and modulation of an impinging radio-frequency (RF) signal. However, the short operational range and low data rates of contemporary BackCom systems render them insufficient on their own to provide ubiquitous connectivity among the plethora of IoT devices. Meanwhile, wireless networks are rapidly evolving towards the smart radio paradigm. Thus, to enhance the coverage range and capacity, reconfigurable intelligent surfaces (RISs) can be incorporated into the existing BackCom systems. RISs employ passive reflective elements to adaptively configure the stochastic wireless environment in a cost-effective and energy-efficient manner. Furthermore, non-orthogonal multiple access (NOMA) can be exploited to improve the spectral efficiency of the BackCom systems. In this paper, we present the design and bit error rate (BER) analysis of an RIS-enhanced NOMA-assisted bistatic BackCom system under Nakagami-m fading channel. Our extensive simulation results reveal the effectiveness of the proposed system over the conventional NOMA-assisted BackCom system without RIS, and demonstrate the impact of various factors, including the power-reflection coefficients, RIS phase-shift designs, number of reflecting elements, RIS location, and split factor, on the BER performance of the proposed RIS-assisted system.**

***Index Terms*—Internet-of-Things (IoT), backscatter communication (BackCom), reconfigurable intelligent surfaces (RISs), non-orthogonal multiple access (NOMA), phase-shift designs, bit error rate (BER).**

I. Introduction

The sixth-generation (6G) of wireless communication aims to fulfill extremely high data rate and ultra-low latency requirements while supporting massive connectivity for empowering the diverse paradigms of wireless communications. The Internet-of-things (IoT) paradigm is envisioned as one of the potential candidates for the provision of ubiquitous connectivity among the massive number of heterogeneous devices [1]. Nevertheless, despite the rapid evolution, the energy management of IoT devices is one of the crucial challenges hindering their large-scale deployment. Conventional battery-based solutions are undesirable for the sustainable operation of IoT nodes in case of deployment in an inaccessible environment and due to the associated cost-prohibitive system maintenance [2]. Consequently, various energy harvesting techniques are under investigation to overcome these challenges. Energy harvesting is a practical and viable approach for IoT networks because of the low energy requirements of IoT devices [2]. In this regard, backscatter communication (BackCom) has emerged as one of the promising energy harvesting solutions for powering the massive number of IoT devices in an energy-efficient and cost-effective manner [3], [4].

BackCom allows the passive backscatter nodes (BSNs) to deliver information by modulating and reflecting the incident radio-frequency (RF) signal via the antenna impedance mismatch. Despite the extensive research on BackCom systems, the issue of limited coverage range and data rates persists [5], [6]. These limitations, along with the stochastic nature of wireless channels, are impeding their large-scale deployment. Therefore, some mechanism is required to support the massive connectivity and high data rate requirements while adapting to the dynamic nature of the wireless channel. In this regard, reconfigurable intelligent surfaces (RISs) have recently emerged as a promising new paradigm for the adaptive configuration of the radio propagation environment [4], [7].

Specifically, an RIS is a planar surface which is composed of a massive number of low-cost passive reflective elements, such as PIN diodes and printed dipole arrays, each capable of intelligently inducing a phase shift and/or amplitude change in the incident signal independently. Thus, the wireless channel between the communication terminals can be reconfigured to achieve the desired channel response. Through intelligent phase-shifts, RIS can either boost the signal to improve the received signal-to-noise ratio (SNR), or attenuate the signal to mitigate the interference. RISs have conformal geometry, hence, they can be easily mounted on environmental objects, such as building facades, walls and ceilings [8].

The aforementioned features of RISs, and their compatibility with the existing wireless systems, make them an ideal candidate to assist BackCom systems [9]. The RIS-assisted

bistatic BackCom system was first studied in [10], where the transmit beamforming vector at the CE, the RIS phase shifts, and the reflection coefficient at the BSNs, were jointly optimized to minimize the transmit power. In [11], performance analysis of RIS-aided BackCom system was studied, and the symbol error probability (SEP) for coherent and random phase-shift designs of RIS was analytically investigated. The authors in [12] investigated the joint optimization of reflection coefficients and RIS phase shifts for an RIS-enhanced NOMA-assisted BackCom system. Moreover, a deep reinforcement learning (deepRL)-based approach for the joint optimization of reflection coefficients and RIS phase shifts for an RIS-assisted ambient BackCom system was presented in [13].

Different from the aforementioned works, in this work, we consider an RIS-enhanced NOMA-assisted bistatic BackCom system. Power-domain NOMA is a promising multiple access technique, which serves multiple users on the same orthogonal resource block, resulting in improved spectral efficiency, massive connectivity, and better user fairness over the OMA techniques [4], [14]. We consider two users per NOMA cluster to ensure low complexity during the successive interference cancellation (SIC) process. In order to better exploit power-domain NOMA (PD-NOMA), the reflection coefficients of the BSNs are assigned different values to establish a higher channel gain difference. The proposed system results in an improved bit error rate (BER) performance as compared to the conventional NOMA-assisted BackCom system. The main contributions of this paper are summarized as follows.

- We propose an RIS-enhanced NOMA-assisted BackCom system, where an RIS assists the backscattering communication between the BSNs and the BR.
- The BER performance of the RIS-enhanced NOMA-assisted bistatic BackCom system is studied under Nakagami-m fading and RIS elements splitting approach.
- Our extensive simulation results show the impact of various factors, namely the transmit SNR, power-reflection coefficients, RIS phase-shift designs, number of reflecting elements, RIS location and split factor, on the BER performance of RIS-enhanced NOMA-assisted BackCom system.

The rest of the paper is organized as follows. In Sec. II, the system model of the proposed RIS-enhanced NOMA-assisted BackCom system is described. Sec. III provides the simulation results to evaluate the performance of the proposed system. Finally, conclusions are presented in Sec. IV.

II. System Model

As illustrated in Fig. 1, we consider an RIS-enhanced NOMA-assisted bistatic BackCom system consisting of a carrier emitter (CE), I backscatter nodes (BSNs), a backscatter receiver (BR), and an RIS with M passive reflective elements. Each passive reflective element has the capability to scatter the impinging signal with an induced phase-shift. We assume that each of the BSNs, BR, and CE is equipped with a single

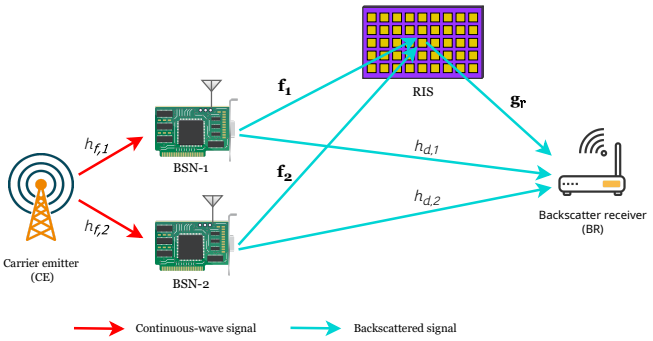

Fig. 1. An illustration of RIS-enhanced NOMA-assisted BackCom system with $I = 2$.

antenna. Let $\mathcal{I} = \{1, \ldots, I\}$ denotes the set of BSNs and $I = |\mathcal{I}|$ denotes the maximum number of BSNs, where $I \geq 2$ and $|\mathcal{I}|$ is the cardinality of set $\mathcal{I}$. Since, the hardware complexity and processing delay due to SIC increases with an increasing number of BSNs per cluster, therefore, in this work, we assume $I = 2$.

A. BackCom Model

The BSNs transmit their data by modulating the continuous-wave (CW) signal generated by the CE. The proposed system has two distinct transmission phases: (i) *forward* or *excitation phase*, where the CE transmits the CW signal to the BSNs; (ii) *backscattering phase*, where the BSNs backscatter the modulated signal towards the BR through both the direct and RIS reflected links.

1) Training Phase: In a single cluster BackCom system with two BSNs, a training phase is employed to distinguish between the strong and weak BSN based on the channel state information (CSI). For this, each BSN backscatters the CW signal towards the BR in a separate time slot with the same value of power reflection coefficient. By comparing the instantaneous CSI, obtained from the received backscattered signals, the BR recognizes the strong/weak BSN. The BSNs then adjust their reflection coefficients, based on their CSI at the BR, to employ PD-NOMA.

2) Operating States: The BSNs in the proposed system operate in one of the two states, either the active state or the energy harvesting state. We assume that the CE continuously transmits the CW signal. In the active state, the BSNs backscatter the modulated signal to the BR, whereas in the energy harvesting state, the BSNs harvest the energy from the CW signal. The harvested energy is stored in a battery to power the internal circuitry and perform sensory functions.

3) BPSK Modulation: The modulation of the incident CW signal is done by varying the antenna impedance of the backscatter device, which in turn changes the value of the reflection coefficient. The BPSK modulation scheme is considered as it aligns with the complexity and energy constraints of the low-power BSNs. For BPSK, the antenna impedance is switched between the two impedance states,

which generates two reflection coefficients with the same magnitude but a phase-shift of 180°.

B. Signal Model

The backscattered signal by the i-th BSN is given by

$$s_i = \sqrt{\Gamma_i P_T} h_{f,i} x_i, \tag{1}$$

where P_T is the CE's transmit power, s_i denotes the backscattered signal of the i-th BSN, Γ_i and x_i denote the reflection coefficient and modulated information symbol of the i-th BSN, respectively. Similarly in (1), $h_{f,i}$ is the fading-free forward channel coefficient, modeled by the propagation path loss $\sqrt{d_{f,i}^n}$, where $d_{f,i}$ is the distance between the CE and the i-th BSN and n is the path loss exponent. Here, the assumption of a fading-free channel model is reasonable since the BSNs are in close proximity of the CE and have a strong line-of-sight (LoS) link with the CE. In addition, since the RIS is deployed close to the BR, therefore, the RIS reflected signal from the CE to the BSNs will be substantially attenuated due to the multiplicative path loss of the reflected link, and hence can be considered negligible. The received signal at the BR is given by

$$y = \sum_{i=1}^{I} \sqrt{\Gamma_i P_T} h_{f,i} \left(\overbrace{\frac{h_{d,i}}{\sqrt{d_{d,i}^n}}}^{\text{direct link}} + \overbrace{\frac{\mathbf{g}_r^{\mathrm{H}} \boldsymbol{\Theta} \mathbf{f}_i}{\sqrt{d_{b,i}^n d_I^n}}}^{\text{RIS reflected link}} \right) x_i + w, \tag{2}$$

where $h_{d,i}$ and $d_{d,i}$ denote the channel coefficient and the distance from the i-th BSN to the BR, respectively. Similarly in (2), $d_{b,i}$ and d_I are the distances from the the IRS to the i-th BSN and CE, respectively, $\mathbf{g}_r \in \mathbb{C}^{M\times 1}$ denotes the channel response matrix between the BR and the RIS, and $\mathbf{f}_i \in \mathbb{C}^{M\times 1}$ is the channel response matrix from the i-th BSN to the RIS. Similarly, $\boldsymbol{\Theta} = \text{diag}\left(\beta_1 e^{j\theta_1}, \beta_2 e^{j\theta_2} \dots \beta_M e^{j\theta_M}\right) \in \mathbb{C}^{M\times M}$ is a diagonal matrix, where $\beta_m \in [0,1]$[1] is the amplitude reflection coefficient and $\theta_m \in \Phi_n$ is the phase-shift induced by the m-th RIS element, where Φ_n denotes the feasible set of phase-shifts. We consider two feasible sets of phase-shifts Φ_1 and Φ_2, where $\Phi_1 = [0, 2\pi)$ is the set of *continuous phase-shifts*, and $\Phi_2 = \{0, \Delta, \dots, (L-1)\Delta\}$ is the set of *discrete phase-shifts*, obtained by uniformly quantizing the interval $[0, 2\pi)$, where $\Delta = 2\pi/L$, and $L = 2^b$ denotes the discrete phase-shift levels which have a b-bit resolution. $w \sim \mathcal{CN}(0, \sigma^2)$ is the additive white Gaussian noise (AWGN) with zero mean and variance σ^2.

It is assumed that all RIS elements reflect the impinging signals independently; consequently, there is no signal coupling in the reflection by the adjacent RIS elements. As such, the RIS reflected link can equivalently be represented as

$$\mathbf{g}_r^H \boldsymbol{\Theta} \mathbf{f}_i = \sum_{m=1}^{M} e^{j\theta_m} g_{r,m} f_{i,m}, \tag{3}$$

[1]We assume that the RIS does not attenuate the amplitude of the incident carrier wave. Hence, in the sequel of this paper, we set $\beta_1 = \beta_2 = \dots = \beta_M = 1$.

where $g_{r,m}$ and $f_{i,m}$ denote the m-th element of $\mathbf{g}_r^H$ and $\mathbf{f}_i$, respectively, and θ_m is the phase of the m-th diagonal element of $\boldsymbol{\Theta}$. In this work, we consider the surface partitioning concept [14], where the total number of RIS elements are split between the *I* BSNs. The distribution of elements is specified by the split factor $\alpha \in [0, 1]$, which is defined as

$$\alpha = \frac{M_1}{M}, \tag{4}$$

where M_1 denotes the number of elements, rounded up to the nearest integer, configured for enhancing the performance of BSN-1 by a coherent combination of the direct and RIS reflected signals at the BR. On the other hand, $M_2 = M - M_1$ are the elements configured for BSN-2 signal. Therefore, for the case of partitioned RIS, the RIS reflected link of the i-BSN can be written as

$$\mathbf{g}_r^H \boldsymbol{\Theta} \mathbf{f}_i = \underbrace{\sum_{m\in C_i} e^{j\theta_m} g_{r,m} f_{i,m}}_{\substack{\text{Coherently optimized} \\ \text{RIS elements for } i\text{-th BSN}}} + \underbrace{\sum_{k\in \overline{C}_i} e^{j\theta_k} g_{r,k} f_{i,k}}_{\substack{\text{Randomly configured} \\ \text{RIS elements for } i\text{-th BSN}}}, \tag{5}$$

where C_i denotes the set of elements configured for the i-th BSN, while $\overline{C}_i$ denotes the set of elements which are not configured for the i-th BSN, and thus randomly combine the signal of i-th BSN. For coherently optimized RIS elements, θ_m is selected as

$$\theta_m = \arg[h_{d,i}] - \arg[g_{r,m} f_{i,m}]. \tag{6}$$

The coherently optimized part of the RIS reflected link can be written equivalently as

$$\sum_{m\in C_i} e^{j\theta_m} \mathbf{g}_{r,m} \mathbf{f}_{i,m} = \sum_{m\in C_i} e^{j \arg[h_{d,i}]} \left|g_{r,m}\right| \left|f_{i,m}\right|. \tag{7}$$

C. Successive Interference Cancellation for Detection

In order to decode the signals transmitted by the BSNs, SIC is carried out at the receiver. The effects of the forward channels $h_{f,i}$'s are compensated in the transmit SNR of both BSNs, and are thus omitted in further analysis. Without the loss of generality, for the case *I* = 2, it is assumed that the BSN-1 has a higher channel gain than the BSN-2 i.e., $\left|h_{b,1}\right| > \left|h_{b,2}\right|$, where $h_{b,i} = \frac{h_{d,i}}{\sqrt{d_{d,i}^n}} + \frac{\mathbf{g}_r^H \boldsymbol{\Theta} \mathbf{f}_i}{\sqrt{d_{b,i}^n d_I^n}}$ is the backward channel of the i-th BSN. Following the SIC scheme, the BR first decodes the data symbol of the strong BSN, i.e., BSN-1, and then subtracts it from the composite received signal to detect the data symbol of the weak BSN, i.e., BSN-2. Hence, the optimal decoding order is in the order of decreasing channel gains.

The receiver decodes the BSN-1's signal using the maximum likelihood detector (MLD), while treating the BSN-2's signal as inter-user interference (IUI). By assuming the availability of perfect CSI at the receiver, the MLD for BSN-1's symbol can be described as

$$\hat{x}_1 = \underset{\tilde{x}_1 \in S}{\arg\min} \left| y - \sqrt{\Gamma_1 P_T} h_{b,1} \tilde{x}_1 \right|^2, \tag{8}$$

TABLE I
SIMULATION PARAMETERS

Parameters	Values
CE's transmit power	P_T = 30 dBm
Nakagami parameters	$m_{h_{d_1}}$ = 5, m_{f_1} = 5 $m_{h_{d_2}}$ = 2, m_{f_2} = 2 m_{g_r} = 3
Number of RIS elements	M = 32
Reflection coefficients	Γ_1 = 0.8 Γ_2 = 0.3
Split factor	α = 0.6
Path loss exponent	n = 2

where $\hat{x}_1$ and $\tilde{x}_1$ denote the estimated data symbol and the possible trial values of x_1, respectively, and $S = \{+1, -1\}$ is the set of all possible constellation points for BSN-1. If the BSN-1's symbol is detected correctly, there is no IUI while decoding BSN-2's symbol. However, in the case of incorrect detection of BSN-1's symbol, a bit error occurs that results in an error propagation from BSN-1, in the form of IUI, during the decoding of BSN-2's symbol. The MLD for BSN-2's symbol can then be described as

$$\hat{x}_2 = \arg\min_{\tilde{x}_2 \in S} \left| (y - \sqrt{\Gamma_1 P_T} h_{b,1} \hat{x}_1) - \sqrt{\Gamma_2 P_T} h_{b,2} \tilde{x}_2 \right|^2, \quad (9)$$

where $\hat{x}_2$ and $\tilde{x}_2$ denote the estimated data symbol and the possible trial value of x_2, respectively. A bit error occurs when $\hat{x}_2 \neq x_2$.

III. Performance Analysis

In this section, we evaluate the performance of the proposed RIS-NOMA-BackCom system through numerical simulations and demonstrate the performance improvement over the conventional NOMA-BackCom system. All wireless channels are assumed to be mutually independent and follow Nakagami-*m* fading distribution, as it provides flexibility in the description of LoS and NLoS links. As in [12], we assume that the CE, RIS, and the BR are located at coordinates $(0, 10)$ m, $(50, 10)$ m, and $(70, 10)$ m, respectively. BSN-1 and BSN-2 are assumed to be located at $(20, 25)$ m and $(20, -5)$ m, respectively. Moreover, in order to ensure successful decoding at the receiver, appropriate values for the reflection coefficients, i.e., Γ_1 and Γ_2, and the split factor, i.e., α, are assumed. Unless mentioned otherwise, the simulation parameters are enlisted in Table I.

A. Performance Enhancement via RIS Integration

In Fig. 2, we evaluate the BER performance against the transmit SNR of each BSN to demonstrate the performance gain achieved by incorporating an RIS into the NOMA-assisted BackCom system. As illustrated in Fig. 2, the RIS-enhanced system outperforms the conventional NOMA-BackCom system without an RIS. This is due to the fact that the direct and

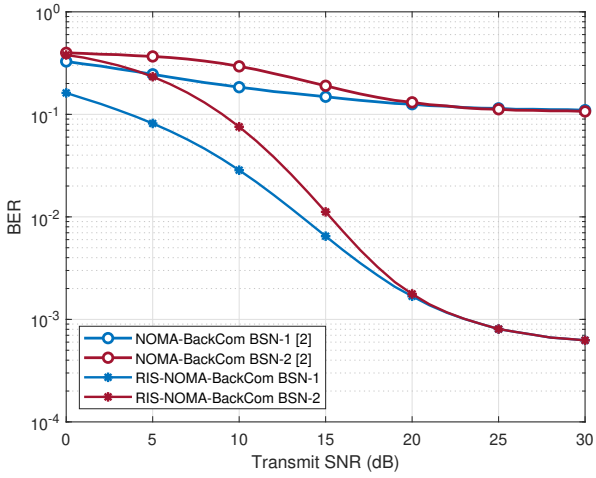

Fig. 2. BER plot of conventional NOMA-BackCom system and RIS-NOMA-BackCom system with M = 24.

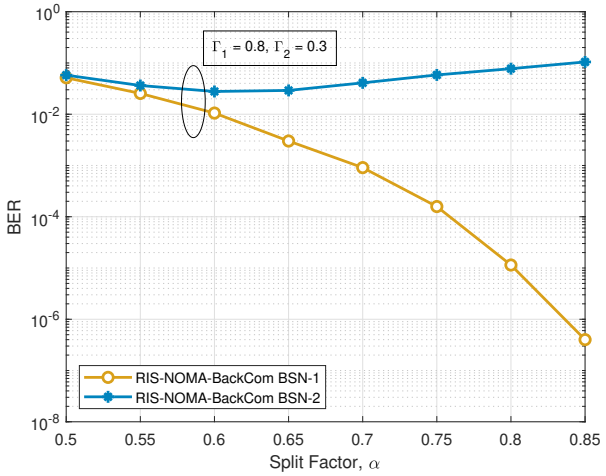

Fig. 3. BER plot for varying split factor, α, with M = 48 and SNR = 5 dB.

RIS reflected signals are added coherently at the BR, which results in improved SNR of the RIS-enhanced system. However, the performance improvement in the low SNR regime is not that eminent due to the severe product-distance path loss experienced by the RIS reflected link.

B. Impact of Elements Splitting

The performance of RIS-enhanced system highly depends on the number of configured RIS elements for each BSN. In this regard, the BER of BSN-1 and BSN-2 is plotted against the split factor, i.e., α, in Fig. 3. It can be observed that the performance of BSN-1 improves with the increase in α since the allocation of more RIS elements to BSN-1 and fewer elements to BSN-2 increases the difference between the received signal strength of both BSNs. This leads to a lower IUI during the decoding of BSN-1's signal, which increases the probability of detecting the BSN-1's data symbol correctly. Consequently, the

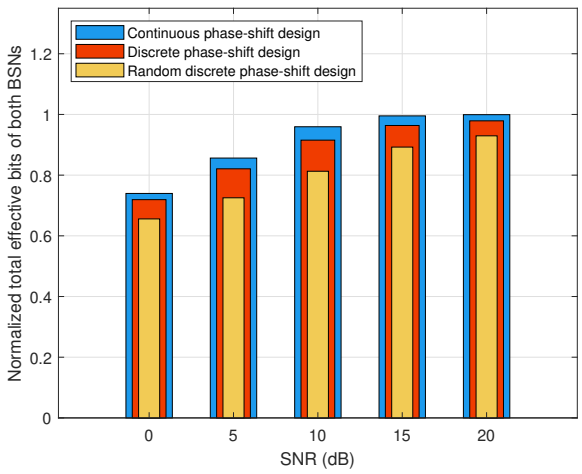

Fig. 4. Effectively decoded bits for BSN-1 and BSN-2 against the transmit SNR for different phase-shift designs and $M = 24$.

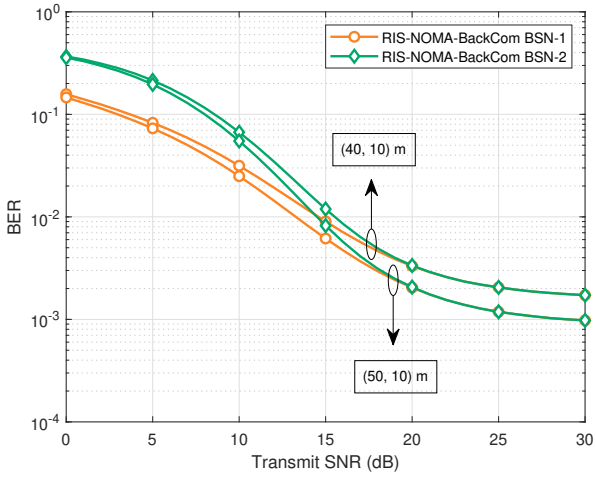

Fig. 5. BER plot for varying location of RIS with M = 24 and α = 0.6.

performance of BSN-2 also improves as there is less probability of error propagation from BSN-1 during BSN-2's decoding.

However, despite the low probability of error propagation from BSN-1, the performance of BSN-2 deteriorates when α is higher than 0.60. This is because the increase in α above the optimal value reduces the strength of the BSN-2's signal significantly, which increases the probability of incorrect decoding. Furthermore, it can be observed that for transmit SNR of 5 dB, the optimal value of a split factor is 0.60 since it provides the lowest BER for both BSNs.

C. Impact of Phase-shift Designs

Fig. 4 compares the performance of the proposed RIS-NOMA-BackCom system for continuous, discrete and random discrete phase-shift designs. In the random discrete phase-shift design, the phase-shift for each element is randomly chosen from the set of discrete phase-shifts, i.e., Φ_2, while in discrete phase-shift design, the optimal phase-shifts are given by

$$\psi_m = \arg\min_{\phi \in \Phi_2} |\phi - \theta_m| , \tag{10}$$

where ψ_m is the optimal value of the discrete phase-shift for the m-th element of RIS.

As illustrated in Fig. 4, the continuous phase-shift approach outperforms the discrete phase-shift designs for a given number of RIS elements and transmit SNR. However, it is infeasible to realize the continuous phase-shifts due to the high hardware cost and complexity [7]. Moreover, the discrete phase-shift design with 1-bit resolution has a better performance than the random discrete phase-shift design with the same resolution. In addition, the performance of discrete phase-shift design can be enhanced by increasing the number of quantization levels.

D. Effect of the RIS Elements and Location

The system performance highly depends on the number of reflective elements and the RIS location. In this regard,

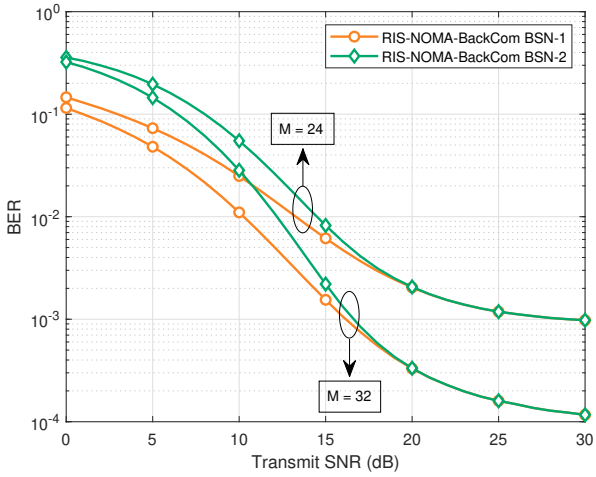

Fig. 6. BER plot for varying number of RIS elements with RIS coordinates $(50, 10)$ m and α = 0.6.

Fig. 5 compares the BER performance for $M = 24$ and RIS located at $(40, 10)$ and $(50, 10)$ m. It can be observed that the BER performance improves by deploying RIS closer to the BR, owing to the reduced path loss of the RIS reflected backward link. The effect of total number of RIS elements on the BER performance for the RIS located at $(50, 10)$ m is illustrated in Fig. 6. As expected, the performance improves when the number of RIS elements is increased. For instance, for 20 dB transmit SNR, the BER performance improves by approximately 80% when RIS elements increase from $M = 24$ to $M = 32$.

E. Effects of the Reflection Coefficients

Fig. 7 illustrates the effect of reflection coefficients on the normalized average of total effectively decoded bits, which corresponds to the sum of non-erroneous transmission of BSNs' bits averaged over the total number of transmitted bits for both

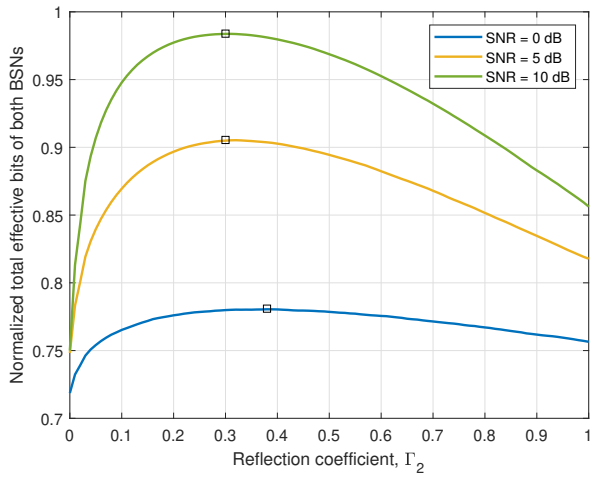

Fig. 7. The normalized average of effectively decoded bits for BSN-1 and BSN-2 against Γ_2 with $\Gamma_1 = 0.8$.

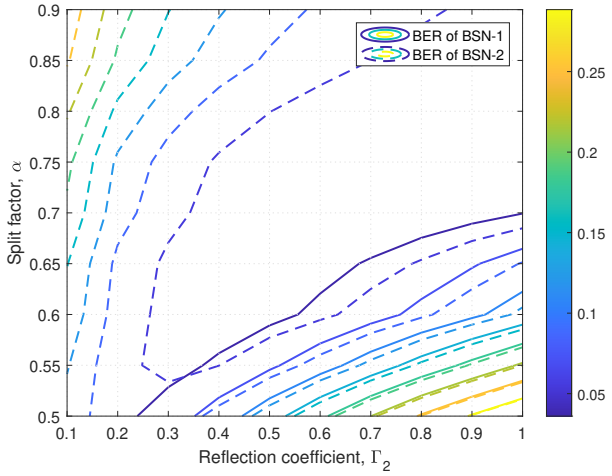

Fig. 8. BER contour plot of BSN-1 and BSN-2 for varying values of Γ_2 and α with $\Gamma_1 = 1$.

BSNs. It can be observed that the optimal Γ_2 for transmit SNRs of 0, 5, and 10 dB is 0.38, 0.30, and 0.30, respectively. Moreover, it can be seen that a greater value of Γ_2 is required to successfully decode the BSNs' signal at low transmit SNRs.

In Fig. 8, a contour plot of BER is plotted by varying the reflection coefficient, Γ_2, and split factor, α, while keeping Γ_1 as 1. It can be observed that for a fixed value of Γ_2, there exists a range of α values which can provide an acceptable BER performance. Moreover, as mentioned before, an increase in Γ_2 deteriorates the system performance due to IUI in the decoding of BSN-1's signal. Moreover, the best BER performance is achieved when Γ_2 is approximately 0.35 and α is 0.6.

IV. CONCLUSION

In this work, we presented an RIS-enhanced NOMA-assisted BackCom system for realizing the high data rate and massive connectivity requirements of 6G IoT networks. Specifically, we studied the BER performance of the RIS-enhanced NOMA-assisted bistatic BackCom system under Nakagami-*m* fading and RIS elements splitting approach. Our extensive simulation results clearly illustrated the performance gain achieved by integrating an RIS and demonstrated that the system performance can be significantly enhanced by increasing the number of reflecting elements, or by selecting the optimal values for split factor and power reflection coefficients without increasing the CE transmit power. Hence, this entails an optimization study as a future work where the split factor and the reflection coefficients can be jointly optimized for the provision of maximum system performance in terms of BER.

ACKNOWLEDGMENT

The work of H. Jung was supported by the Ministry of Science and ICT, Korea under the Information Technology Research Center support program (IITP-2021-0-02046).

REFERENCES

[1] D. C. Nguyen, M. Ding, P. N. Pathirana, A. Seneviratne, J. Li, D. Niyato, O. Dobre, and H. V. Poor, "6G Internet of Things: A comprehensive survey," *IEEE Internet of Things Journal*, vol. 9, no. 1, pp. 359–383, 2022.

[2] A. W. Nazar, S. A. Hassan, H. Jung, A. Mahmood, and M. Gidlund, "BER analysis of a backscatter communication system with non-orthogonal multiple access," *IEEE Transactions on Green Communications and Networking*, vol. 5, no. 2, pp. 574–586, 2021.

[3] J. Guo, X. Zhou, S. Durrani, and H. Yanikomeroglu, "Design of non-orthogonal multiple access enhanced backscatter communication," *IEEE Transactions on Wireless Communications*, vol. 17, no. 10, pp. 6837–6852, 2018.

[4] S. Basharat, S. Ali Hassan, H. Pervaiz, A. Mahmood, Z. Ding, and M. Gidlund, "Reconfigurable intelligent surfaces: Potentials, applications, and challenges for 6G wireless networks," *IEEE Wireless Communications*, vol. 28, no. 6, pp. 184–191, 2021.

[5] A. W. Nazar, S. A. Hassan, and H. Jung, "BER analysis of a NOMA enhanced backscatter communication system," in *GLOBECOM 2020 - 2020 IEEE Global Communications Conference*, 2020, pp. 1–6.

[6] J.-P. Niu and G. Y. Li, "An overview on backscatter communications," *Journal of Communications and Information Networks*, vol. 4, no. 2, pp. 1–14, 2019.

[7] Q. Wu and R. Zhang, "Towards smart and reconfigurable environment: Intelligent reflecting surface aided wireless network," *IEEE Communications Magazine*, vol. 58, no. 1, pp. 106–112, 2020.

[8] Q. Wu, S. Zhang, B. Zheng, C. You, and R. Zhang, "Intelligent reflecting surface-aided wireless communications: A tutorial," *IEEE Transactions on Communications*, vol. 69, no. 5, pp. 3313–3351, 2021.

[9] S. Basharat, S. A. Hassan, A. Mahmood, Z. Ding, and M. Gidlund, "Reconfigurable Intelligent Surface-Assisted Backscatter Communication: A New Frontier for Enabling 6G IoT Networks," *arXiv preprint arXiv:2107.07813*, 2021.

[10] X. Jia, J. Zhao, X. Zhou, and D. Niyato, "Intelligent reflecting surface-aided backscatter communications," in *GLOBECOM 2020 - 2020 IEEE Global Communications Conference*, 2020, pp. 1–6.

[11] W. Zhao, G. Wang, S. Atapattu, T. A. Tsiftsis, and X. Ma, "Performance analysis of large intelligent surface aided backscatter communication systems," *IEEE Wireless Communications Letters*, vol. 9, no. 7, pp. 962–966, 2020.

[12] J. Zuo, Y. Liu, L. Yang, L. Song, and Y.-C. Liang, "Reconfigurable intelligent surface enhanced NOMA assisted backscatter communication system," *IEEE Transactions on Vehicular Technology*, vol. 70, no. 7, pp. 7261–7266, 2021.

[13] X. Jia and X. Zhou, "IRS-assisted ambient backscatter communications utilizing deep reinforcement learning," *IEEE Wireless Communications Letters*, vol. 10, no. 11, pp. 2374–2378, 2021.

[14] B. Tahir, S. Schwarz, and M. Rupp, "Outage analysis of uplink IRS-assisted NOMA under elements splitting," in *2021 IEEE 93rd Vehicular Technology Conference (VTC2021-Spring)*, 2021, pp. 1–5.